Analytica Chimica Acta 1105 (2020) 178–186

Contents lists available at ScienceDirect

Analytica Chimica Acta

journal homepage: www.elsevier.com/locate/aca

In silico maturation of affinity and selectivity of DNA aptamers against aflatoxin B_1 for biosensor development

Maryam Mousivand [a, b], Laura Anfossi [c, f], Kowsar Bagherzadeh [d, e], Nadia Barbero [c, f], Amir Mirzadi-Gohari [a], Mohammad Javan-Nikkhah [a, *]

[a] Department of Plant Protection, College of Agricultural Sciences & Engineering, University of Tehran, Karaj, 31587-77871, Iran
[b] Microbial Biotechnology Department, Agricultural Biotechnology Research Institute of Iran, Agricultural Research, Education and Extension Organization, 3135933151, Karaj, Iran
[c] Department of Chemistry and NIS Interdepartmental Center, University of Turin, Via Pietro Giuria 5, 7, 10125, Turin, Italy
[d] Eye Research Center, The Five Senses Institute Rassoul Akram Hospital, Iran University of Medical Sciences, Tehran, Iran
[e] Razi Drug Research Center, Iran University of Medical Sciences, Tehran, Iran
[f] Department of Chemistry, University of Turin, Via Giuria, 5, I-10125, Turin, Italy

HIGHLIGHTS

- An in silico strategy was developed to improve affinity and selectivity of aptamers over aflatoxin B_1.
- Fluorescent anisotropy and unmodified gold nanoparticles assays faithfully confirmed insilico results.
- A new functional aptamer for aflatoxin B_1 was identified through computational studies.
- A novel fluorescent anisotropy aptamer assay was developed for functional validation of aflatoxin B_1 aptamers.
- A simple pipeline for three dimensional modeling of ssDNA aptamers was proposed.

GRAPHICAL ABSTRACT

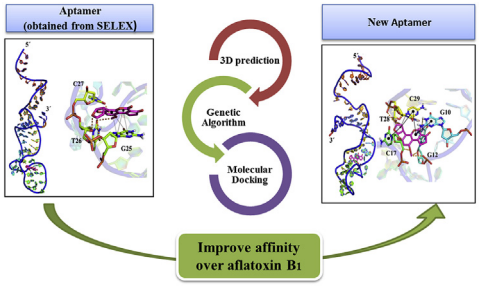

ARTICLE INFO

Article history:
Received 8 November 2019
Received in revised form
17 January 2020
Accepted 21 January 2020
Available online 24 January 2020

Keywords:
Aflatoxin B_1
Aptamer
Molecular docking
Fluorescent anisotropy
Genetic algorithm
Gold nanoparticles

ABSTRACT

A high affinity and selectivity DNA aptamer for aflatoxin B_1 (AFB_1) was designed through Genetic Algorithm (GA) based in silico maturation (ISM) strategy. The sequence of a known AFB_1 aptamer (Patent: PCT/CA2010/001292, Apt1) applied as a probe in many aptasensors was modified using seven GA rounds to generate an initial library and three different generations of ss DNA oligonucleotides as new candidate aptamers. Molecular docking methodology was used to screen and analyze the best aptamer–AFB_1 complexes. Also, a new pipeline was proposed to faithfully predict the tertiary structure of all single stranded DNA sequences. By the second generation, aptamer Apt1 sequence was optimized in the local search space and five aptamers including F20, g12, C52, C32 and H1 were identified as the best aptamers for AFB_1. The selected aptamers were applied as probes in an unmodified gold nanoparticles-based aptasensor to evaluate their binding affinity to AFB_1 and their selectivity against other mycotoxins (aflatoxins B_2, G_1, G_2, M_1, ochratoxin A and zearalenone). In addition, a novel direct fluorescent anisotropy aptamer assay was developed to confirm the binding interaction of the selected aptamers over AFB_1. The

* Corresponding author.
E-mail addresses: laura.anfossi@unito.it (L. Anfossi), jnikkhah@ut.ac.ir (M. Javan-Nikkhah).

https://doi.org/10.1016/j.aca.2020.01.045

ISM allowed the identification of an aptamer, F20, with up to 9.4 and 2 fold improvement in affinity and selectivity compared to the parent aptamer, respectively.

1. Introduction

Aflatoxin B_1, known as the most potent carcinogen, was produced mainly by *Aspergillus flavus* and *A. parasiticus*. Chemically, the AFB_1 molecule contains two furan rings relating to toxicity and a highly substituted coumarin relating to carcinogenicity [1] and is listed as Group 1 human carcinogens [2]. Due to the low level permission of AFB_1 (2–5 μg kg^{-1}) regulated by different countries and the complexity of the food sources, it is important to develop sensitive and rapid methods for AFB_1 detection to ensure food safety and human health. The chromatographic [3,4] and immunological methods [5,6] are commonly applied for AFB_1 detection. Although these techniques provide sufficient sensitivity and accuracy, some disadvantages make it difficult to apply them for on-site detection. Chromatography-based methods require expensive instruments, well-trained professionals and tedious procedures. Advantages of antibody-based immunoassays are rapidity and simplicity; however their practical application is often hampered by the difficulty of producing antibodies and requiring long reaction time and multiple incubation and washing steps [7]. The increasing demand for accurate, fast and portable tools to determine of mycotoxins for on-site and real-time applications caused to develop different biosensors. Although antibodies are the gold standard for use in biosensors as a recognition element but aptamers have been increasing in popularity due to their advantages including small size, simple synthesis, low cost, easy modification and target diversity [8].

Aptamers are single-stranded oligonucleotides that can specifically bind to a target molecule and are obtained from a random library through an iterative in vitro process called SELEX (systematic evolution of ligands via exponential enrichment) [9]. Considering the low diversity of the initial library and the loss of potential high affinity aptamers during biased iterative PCR, the success rate of SELEX has been estimated approximately 50% [10].

In Silico Maturation (ISM) as a post SELEX process is a successful strategy for improving functions of aptamers based on Genetic Algorithm (GA). This process used the three GA operations, including selection, crossover and mutation [11], to evolve improved aptamers from promising parent sequences through an iterative process of in silico sequence modifications followed by in vitro evaluation. The first application of the ISM-based GA to improvement of aptamer functionality has been reported in 2005 [13] for screening thrombin-inhibiting DNA aptamer. Although, the ISM strategy has been performed to find high affinity aptamers for several targets without recurring to the SELEX process [12–14], but in silico methods have not been applied to improve aptamer affinity against mycotoxins until now.

In fact, selection, characterization and improvement of aptamers over mycotoxins as carcinogenic and toxic compounds are less compared to other larger target molecules such as proteins and cell because of their molecular weights. The drastic size difference between the small molecules and aptamers is a main challenge to select, characterize, and apply aptamers for them through conventional SELEX procedures [15]. Regarding to the difficulties in experimentally identification of high functional aptamers over small molecules, in silico methods can be applied as effective complementary options for identifying or improving of aptamers over them with no cost.

Although ISM has a smaller library than the SELEX process, all sequences in each generation (~10–50 sequences) must be synthesized and evaluated [16]. Therefore the ISM process still is expensive, tedious and time consuming for high-throughput screening. Also it is not possible to determine structural features of aptamer-ligand complex for each GA run to select the best parent aptamers or modify them for the next generation. In silico screening undoubtedly plays an important role in identifying all interaction between aptamer-ligand complexes in cost- and time-effective ways [17].

Computational docking tools such as AutoDock and DOCK programs can be successfully applied to screen a library of nucleic acid molecules to find receptors with the highest binding affinity to a desired small molecule [18]. One of the main problems in molecular docking of DNA aptamers and their targets is lacking the 3D structure prediction tools for ss DNA molecules. Recently a new pipeline was proposed to predict the three dimensional modeling of single stranded DNA for aptamer-based biosensors [19].

Furthermore, standardized analytical methodologies for the characterization of small molecule-binding aptamers are not available, because of the low sensitivity of binding assays [20]. One of the most simple and effective ones is the unmodified gold nanoparticles (AuNPs) based aptasensor, which enables a visible detection by the naked eye [21]. The fluorescent anisotropy aptamer assay (FAAA) is known as a sensitive and reliable strategy in small molecule-aptamer evaluation as well. Direct format of FAAA can be used to evaluate the complex formation between the aptamer and a small fluorescent target [22].

Recently, a Canadian company patented a specific aptamer to AFB_1 and zearalenone, here known as Apt1 [23], applied in the construction of several aptasensors [24–27]. In this study, we described a novel and successful post-SELEX procedure combining ISM strategy and molecular docking to introduce high affinity and selectivity AFB_1-targeting aptamers for biosensing applications based on Apt1 sequence. In addition, we proposed an effective and simple pipeline for three dimensional modeling of ssDNA aptamers as input structures in molecular simulations. The in silico results were evaluated on the basis of affinity and selectivity using colorimetric AuNPs-based aptasensor. Moreover, we highlight the potential of direct FAAA methodology as a rapid, accurate and homogeneous analysis for detection of binding interaction between aptamers and intrinsic fluorescent small molecules such as AFB_1.

2. Material and methods

2.1. In silico maturation of aflatoxin B_1 aptamer

2.1.1. Generation of the initial library

The Apt1 aptamer sequence was applied as parent sequence to produce the initial library using different GA operators. The library consisted of four groups of sequences including L1, L2, L3 and L4 generated by one and two point mutations, different crossing over (single point, double point and uniform cross over), one point mutation and two points mutation, respectively. All GA processes were implemented using MATLAB software (R2013B) with constant crossing over percentage (0.8) and mutation rate (0.02). The

sequences belonging to each group was used as parents to generate the next groups.

2.1.2. Improvement of binding affinity of aflatoxin B_1 aptamer

GA based-ISM approach combined with molecular docking to improve the binding affinity of Apt1 over AFB_1. The binding affinity of the initial library, including 65 sequences, was screened through molecular docking to produce three different generations as follow. According to the docking results, the top sequences of the initial library were selected, replicated with different appearance rates depending on the docking results and were paired with each other randomly as parents to produce the first generation (G1). The sequences were modified with single point, double point and uniform crossing over through Roulette Wheel Selection method implemented using GA for producing 24 new sequences as G1. To produce the second generation (G2), the top G1 and library sequences were replicated with different appearance rates depending on the docking results. A one-base mutation was randomly introduced to the sequences to produce a set of 24 new sequences as G2. The third generation (G3) consists of 24 new sequences obtained from the library, G1 and G2 top sequences replicated according to the docking results and modified using two bases mutations. After three cycles of GA, the sequences with the highest affinity to AFB_1 were selected (Scheme 1). The selectivity of the selected aptamers for 6 different mycotoxins including aflatoxin B_2 (AFB_2), aflatoxin G_1 (AFG_1), aflatoxin G_2 (AFG_2), aflatoxin M_1 (AFM_1), ochratoxin A (OTA) and zearalenone (ZEN) were evaluated using molecular docking as well.

2.1.3. Prediction of the aptamer secondary structures

Secondary structures of all sequences in the initial library and the three new generations were predicted using Mfold web server (http://mfold.rna.albany.edu/?=mfold) [28]. The most thermodynamically stable structures were predicted at 37 °C and at ionic concentration of 1 M of Na^{+}, 0 M of Mg^{2+}. All sequences were considered as linear and only fold configurations within 5% from the minimum free energy were computed.

2.1.4. Prediction and validation of 3D-structures

The construction of the 3D-structure from the aptamer sequence consists of a pipeline with three main steps. At first, the secondary structure of each sequence was predicted using Mfold server. The predicted secondary structures were converted into equivalent 3D ssRNA models using RNA Composer server [29]. The obtained tertiary structures of RNA were minimized using steepest descent algorithm implemented in Chimera 1.11.2 [30]. In the third step, the minimized ssRNA molecules were translated to ssDNA by converting uracil residues to thymine and replacing the ribose sugar backbone with deoxyribose. The final ss DNA models were refined to 0.00001 kcal $mol^{-1}Å^{-1}$ using CHARMM27 force field implemented in Molecular Operating Environment [31].

The accuracy of the procedure was evaluated by predicting 22 ssDNA sequences from Protein Data Bank (PDB) database with NMR solved structures. The root mean square deviation (RMSD) of the sugar-phosphate backbone of NMR solved structures and the ones predicted using the proposed pipeline was compared using VMD [32] to determine the similarity degree and method confidence. The obtained results were also compared to those obtained through the method of Jeddi and Saiz [19] as well.

2.1.5. Docking methodology

AFB_1 binding affinity and selectivity of the designed ssDNA aptamers was estimated with the grid-based ligand docking program AutoDockTools (ADT) 1.5.4 package [33]. The refined 3D predicted structures of aptamers were kept as rigid receptors while AFB_1 was considered as a flexible ligand with only one rotatable bond. To cover the whole active sites in folding aptamers, two same grid boxes of 126 × 126 × 126 Å (x, y, and z) were created separately with the spacing of 0.375 Å. All docking simulations were setup for 100 genetic algorithm runs using the Lamarckian genetic algorithm conformational search, with the population size of 150, 2500000 maximum numbers of energy evaluations and 27000 generations per run. The best complexes were scored and selected according to the molecular docking results including binding energy, inhibitory constant (k_i), type of favorable interactions (mainly hydrogen bonds, hydrophobic and electrostatic interactions) and binding sites.

2.1.6. Graphical representation

The graphical representation of aptamer-AFB_1 complexes and their interactions generated using PyMol [34], MOE and Discovery Studio 4.1 [35].

2.2. Experimental assays

To validate the in silico procedure and develop a new aptasensor, the selected aptamers were evaluated experimentally as follows.

2.2.1. Reagents and apparatus

All the reagent grade chemicals, including Gold (III) chloride trihydrate, sodium citrate ($C_6H_5Na_3O_7$), sodium chloride (NaCl), magnesium chloride ($MgCl_2$), calcium chloride ($CaCl_2$), Potassium chloride (KCl), Tris–base, HCl, HNO_3 and all mycotoxins were purchased from Sigma-Aldrich (St. Louis, MO, USA). The water used throughout all experiments was purified by a Milli-Q system at 18 MΩ. The aptamers were synthesized by TAG Copenhagen A/S (Denmark) at synthesis scale of 0.2 μmol. The optical density (OD)

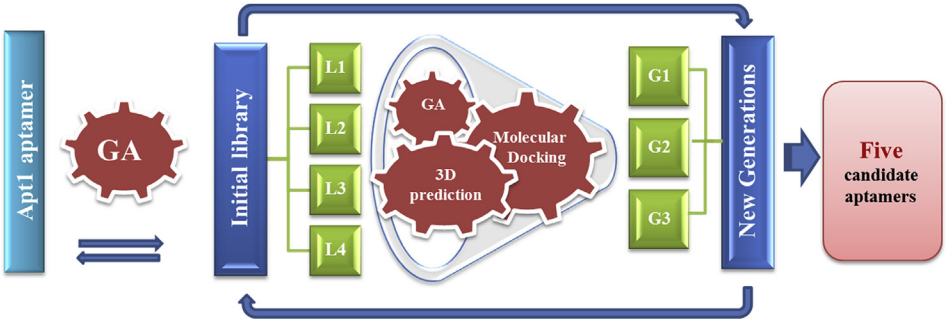

Scheme 1. The Genetic Algorithm (GA) based -in silico maturation strategy combined with molecular docking to improve the affinity of Apt1 aptamer versus aflatoxin B_1.

of gold nanoparticles was measured on a Multiskan Microplate Reader (ThermoFisher, USA). Fluorescence anisotropy and fluorescence intensity was recorded using an LS55 PerkinElmer spectrofluorimeter.

2.2.2. Preparation of gold nanoparticles

AuNPs were synthesized with an average particle diameter of 13 nm using the citrate reduction method [36]. The AuNPs were characterized using a UV–visible spectrometer (Varian Cary 1E from Agilent, USA) and showed a plasmonic resonance (SPR) band centered at 520 nm (details in the Supporting Information).

2.2.3. Colorimetric aptasensing of AFB_1

According to the optimal procedure (details in the Supporting Information), 50 μl of aptamer (400 nM) and 50 μl of AFB_1 in various concentrations (0, 0.1, 0.2, 0.5, 1, 2 and 5 ng ml^{-1}) were incubated for 5 min at room temperature in microplate wells. Then 50 μl of AuNPs (~13 nm) was added to each microplate well and incubated for further 5 min. Immediately after adding 10 μl of NaCl (1 M), the color and optical density (OD) shift were recorded using a digital camera and a microplate reader provided with filter at 620 and 540 nm. The sensitivity of different aptamers was determined by plotting OD ratio (620/540 nm) against AFB_1 concentration. The dissociation constant (K_D) was determined by one site specific binding equation through nonlinear regression analysis using the programs Origin pro 8.6.1 and GraphPad Prism 8.0 .0.

Under the optimal conditions, the selectivity of the aptamers was evaluated against other mycotoxins including AFB_2, AFG_1, AFG_2, AFM_1, OTA and ZEN at the concentration of 10 ng ml^{-1}. The ratio 620/540 nm of the different aptamers was calculated for each mycotoxin, normalized based on maximum value and expressed as selectivity percentage.

2.2.4. Fluorescent intensity (FI) and direct fluorescent anisotropy aptamer assay (FAAA)

The change of the anisotropy signal and fluorescent intensity between AFB_1 free in solution and AFB_1 bound to the aptamer was recorded with excitation at 429 nm and emission at 365 nm. In fluorescence anisotropy, slits for the excitation and emission were both set at 10 nm and integration time was 5 s. The selected aptamers were prepared in ultra-pure water at 9 different concentrations (0–1000 nM) and heated at 90 °C for 5 min prior to use. The AFB_1 solution was prepared in binding buffer (consisting of 20 mM Tris–HCl (pH 7.6), 100 mM NaCl, 2 mM $MgCl_2$, 5 mM KCl, 1 mM $CaCl_2$) at the concentration of 10 ng ml^{-1}. For both the assays, FI and FAAA, 100 μl of the aptamer solution and 100 μl of AFB_1 solution were mixed and incubated for 5 min at RT before measuring fluorescent intensity and anisotropy. The anisotropy signal and fluorescent intensity were plotted versus the aptamer concentration and the K_D values were determined as described previously using the programs Origin pro 8.6.1 and GraphPad Prism 8.0 .0 [20,37].

3. Results and discussion

3.1. Thermodynamic properties of the candidate aptamers

The initial library consisted of 65 ssDNA oligonucleotides and contained three different types of secondary structures including simple hairpin loop (H-loop), internal loop (I-loop) and multi-branch loop (MB-loop). The three different generations of aptamers had more diverse secondary structures and contained pseudo knot structures as well (Fig S1). The minimum free energy of secondary structure formation (ΔG) in the initial library and different generations were in the range −2.20 to −11.30 and −1.50 to −11.30 kcal mol^{-1}, respectively. Aptamer Apt1 displayed H- loop structure (Fig S2) and its ΔG was estimated at −8.01 kcal mol^{-1}. The results revealed that different operators of GA can successfully create a virtual library and different generations with high diversity in the secondary structures and thermodynamic properties.

3.2. Three dimensional modeling

Typically a virtual screening requires knowledge of 3D structure of receptor and the ligand molecules. The lack of computational tools for three dimensional modeling of ssDNA molecules and the difficulties in experimentally determine 3D structures of all sequences in a library have led researchers to seek reliable predicted methods. By some modifications, we used a pipeline previously reported for the first time by Jeddi and Saiz [19] to predict the three dimensional modeling of ssDNA aptamers. The main prediction steps, which consist of: (i) building secondary structures, (ii) constructing refined equivalent 3D ssRNA models, and (iii) translating the 3D ssRNA models into ssDNA, were carried out as reported. However, we used the RNAComposer/Chimera instead of Assemble2/Chimera in step (ii). Also, instead of VMD program, we used MOE package to convert ssRNA models into equivalent ssDNA 3D structures and refine them. The modified pipeline was validated through 3D modeling of 22 ssDNA aptamers with known structures. The RMSD values of the designed models was calculated with respect to the experimentally determined structures and compared to those predicted by Jeddi et al. [19], as well. The RMSD results showed that the new pipeline predicted 63.63% of structures more accurately than the pipeline proposed by Jeddi et al. (Fig. 1, Table S7). Then, the 3D structures of all new aptamers were predicted using our pipeline and used for molecular docking study.

3.3. In silico maturation of binding affinity to AFB_1 using GA

Molecular docking was used to predict the binding energy, binding sites and mode of interactions between AFB_1 and the 137 candidate aptamers including 65 and 72sequences from initial library and three different generations respectively. The predicted binding energies of ssDNA aptamers in the initial library and different generations were in the range −4.19 to −6.6 (Table S1) and −4.29 to −7.14 kcal mol^{-1} (Table S2, S3, S4) respectively.

The mode of interaction between Apt1 and AFB_1 was identified as an intercalation between the base pairs with docking energy of −5.21 kcal mol^{-1}. The binding residues of Apt1(G25, T26 and C27 in the loop region) interacted with the furan and coumarin moieties of AFB_1 through hydrogen bonding and hydrophobic interaction. These results are in accordance with those reported by Ref. [27] that experimentally confirmed the crucial role of the nucleotides in the loop region of Apt1 for affinity binding. This further confirmed the validity of the 3D-structure prediction and the docking methods used in this work.

Most of the 'top' sequences in the initial library and new generations had simple H-loop structures (Fig S1) and their ΔG were equal or lower than that of Apt1. The findings seem to be consistent with another research, which found the candidate aptamers in RNA pools displayed simple secondary structures and lower ΔG compared to other sequences in a random library [38].

Also, the binding sites of H-loop aptamers (71.4%) were mainly located in the same loop region while in 74.6% of MB-loop aptamers was located outside of loop region. Typically, the unpaired residues participate in target recognition as binding sites because they are more flexible and have more available donor or acceptor atoms [39]. Interestingly, the docking results and secondary structure analysis revealed that the loop size can affect the binding affinity of H-loop aptamers: increasing or decreasing the loop size over the

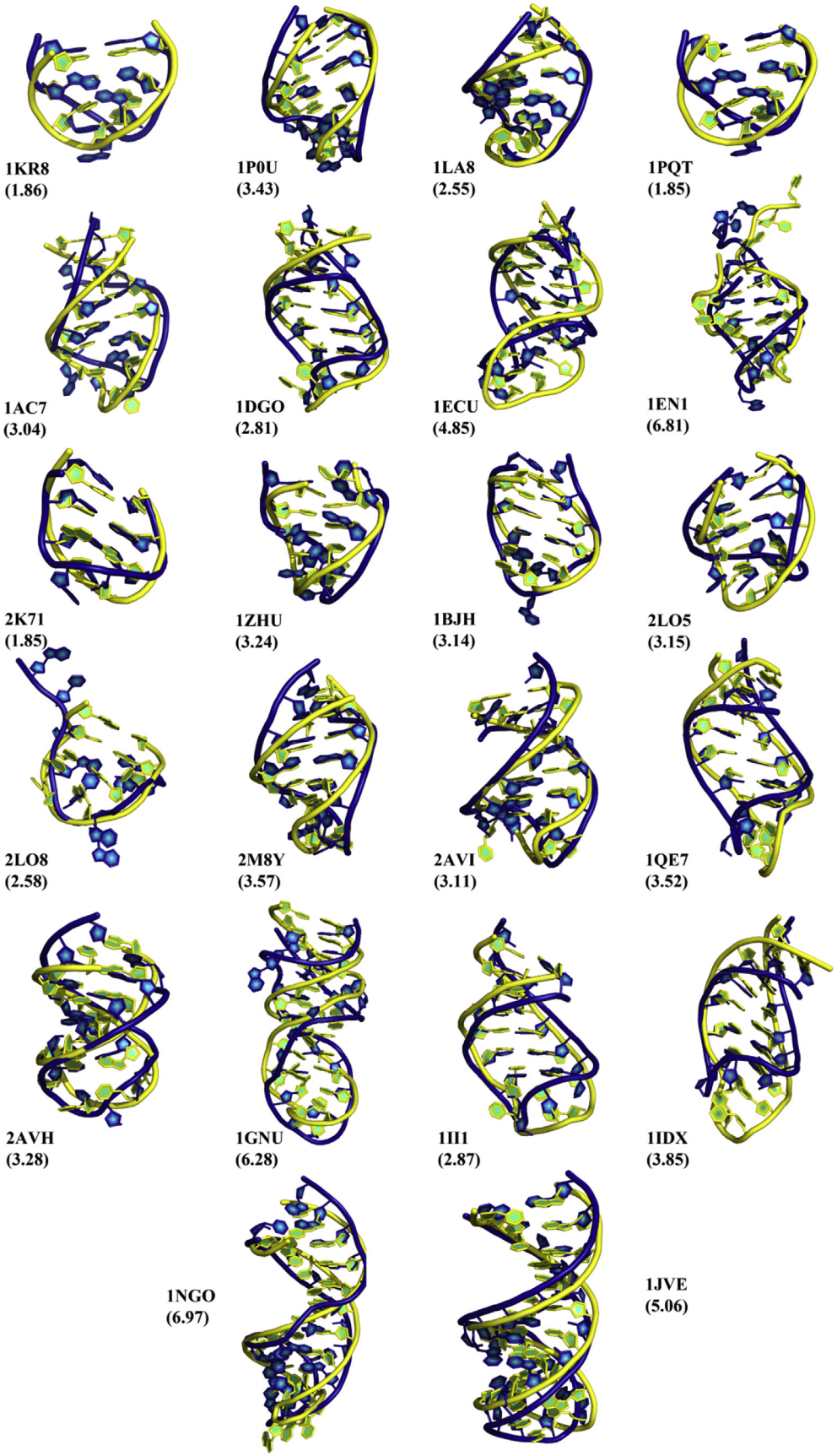

Fig. 1. Alignment of the 3D structures predicted by our pipeline (RMSD1, in blue) and the corresponding experimental ones obtained from PDB (RMSD2, in yellow) for the 22 ssDNA structures. The PDB ID and RMSD values (Å) are presented as label and in parenthesis, respectively. (For interpretation of the references to color in this figure legend, the reader is referred to the Web version of this article.)

optimal size (12–20 bases) caused a decreasing in the binding affinity to AFB_1.

According to the results, the average binding energy of candidate aptamers gradually decreased from the initial library to G2, while significantly increased in the third generation. Also, the thermodynamic analysis revealed that the complexity of the structures and ΔG increased in G3 compared to other two generations and to the initial library. It seems that the aptamer sequences have been optimized in the local search after 7 GA rounds and further modification probably caused divergence of the sequence resulting in the loss of functionality.

Among the top sequences from the initial library, aptamers C52 and C32 exhibited the highest affinity to AFB_1. The binding energy of C52 and C32 aptamers were estimated as −6.6 and −6.06 kcal mol^{-1}, respectively. The binding pocket of aptamer C32, located in the loop region, interacted with AFB_1 through hydrogen bonding and hydrophobic interaction. The binding residues of aptamer C52 was in the non-loop region and interacted with AFB_1 through hydrogen bonding, hydrophobic and electrostatic interactions. Modes of interaction of aptamers C32 and C52 with furan, coumarin and carbonyl groups of AFB_1 were intercalation and minor groove binding, respectively.

Aptamers g12, F20 and H1, with H-loop structure and docking energy of −6.1, −7.14 and −6.58 kcal mol^{-1}, respectively, showed the highest affinity to AFB_1 in G1, G2 and G3, respectively. The binding sites of aptamers g12 and H1were located in the non-loop region and interacted with AFB_1 through hydrogen bonding, hydrophobic and electrostatic interactions. Docking results revealed that the furan ring, coumarin and carbonyl groups of AFB_1 interacted with aptamers g12, F20 and H1 through minor groove binding.

Compared to all other 'top' aptamers, aptamer F20 showed the highest affinity to AFB_1 and was identified as a local optimum of the defined search space. The binding sites of aptamer F20 was located in the loop and stem regions and interacted with AFB_1 through hydrogen bonding and hydrophobic interaction. Also, parallel-displaced arene-arene interactions between residue G12 and delta lactone group of AFB_1 played a significant role in enhancing complex stability.

Basing on the thermodynamic properties and docking analysis, five aptamers, including C52, C32, g12, F20 and H1 were selected as the best candidate aptamers (Fig. 2; Fig S3; Table S5) for being evaluated by experimental work. The aptamer Apt1 was used as a control in the experimental part of the work.

3.4. Unmodified AuNPs-based colorimetric assay

The visible or detectable coloring shift of AuNPs from red (dispersed state) to purple (aggregation induced typically through the addition of salt) is the basis of the unmodified AuNPs colorimetric assay. It has been found that ssDNA (such as aptamers) easily adsorbs onto the surface of AuNPs and stabilizes them against salt induced aggregation. However, upon the addition of AFB_1, the aptamer experiences a structural change and loses its role as a stabilizer. As a result, high-salt content causes the aggregation of unshielded AuNPs with an appreciable color change, and a measurable shift of the AuNPs SPR band [21].

The affinity of the new aptamers (C52, C32, g12, F20 and H1) and Apt1 as control towards AFB_1 was evaluated using the unmodified AuNPs-based colorimetric assay under optimized conditions (details in the Supporting Information). While increasing the concentration of AFB_1, a gradual decrease of the optical density of AuNPs was observed at 540 nm (disperse AuNPs) under high-salt content, while a corresponding increase was recorded at 620 nm (aggregated AuNPs). The SPR shift confirmed that the aptamers underwent structural changes due to the interaction with AFB_1 and less shielded nanoparticles began to aggregate. The ratio 620/540 nm was plotted versus AFB_1 concentration. For all aptamers, the range of linear dependence of the signal from AFB_1 concentration was found to be comprised between 0.05 and 5 ng ml^{-1}, thus envisaging also the direct application of the method to detect AFB_1 in food, according to legal requirements of the European Union [40]. The K_D values of the investigated aptamers were in the range 8.70E+00 to 4.98E+01 nM (Fig S4, Table 1). The highest affinity was calculated for aptamer F20 which showed 3.24fold improved affinity to AFB_1 compared to the control Apt1. Comparing the experimental and in silico affinity rate revealed approximately 70% of accordance (Table 1). Therefore, the in silico approach confirms its applicability as an advantageous tool for improving aptamer structure and function in order to design aptamer-based biosensors.

3.5. Experimental and in silico evaluation of aptamer selectivity

Selectivity of the binding to the target is one of the most important factors for sensor design. Due to the difficulty of experimentally evaluating different aptamers over various structurally related compounds, an in silico approach can be helpful for selecting high specific aptamers. Here, the selectivity of C52, C32, g12, F20, H1 and Apt1 aptamers over different mycotoxins, including AFB_1, AFB_2, AFG_1, AFG_2, AFM_1, ZEN and OTA, was studied using molecular docking (Fig S6-S11). The results were analyzed based on the binding energy value, binding sites and type of interactions, which mainly included hydrogen binding, electrostatic and hydrophobic interactions (Table S6). To validate the in silico approach, the selectivity of the aptamers against the mycotoxins was investigated also experimentally by the colorimetric assay. According to the experimental results, all aptamers showed the highest affinity towards AFB_1. Aptamer F20 had the highest selectivity to AFB_1 compared to other aptamers and its selectivity over six mycotoxins improved two-folds compared to that of aptamer Apt1. Also, the selectivity of aptamers H1, g12 and C52 over the other mycotoxins was approximately 1.5 times that of Apt1. The Apt1 exhibited the highest affinity to AFB_2, AFG_2 and ZEN compared to other aptamers. This finding appears to be in line with results of other researches that reported the Apt1 had cross reactivity to ZEN [23], AFG_2 and AFM_1 [24]. The aptamer C32, showed the highest selectivity to AFM_1 and a similar selectivity profile as for Apt1 (Fig. 3).

In both in silico and experimental methods, the aptamers were sorted according to their selectivity against each mycotoxin and compared with each other. There was a good correlation between in silico and experimental results, where 54.19% of docking results were confirmed by the experiment. The binding sites of various mycotoxins on each aptamer overlapped approximately 76%. Due to the structural similarity of mycotoxins, especially aflatoxins, this was expected and further confirmed the validity of the docking methodology.

3.6. Fluorescent intensity and direct fluorescent anisotropy aptamer assay

Despite increasing of specific aptamers developed for small molecules, there are not standard binding assays to convert aptamer-target interactions into sufficiently sensitive signals. The confirmation of aptamer – target binding using more than one analytical method is known as a successful strategy especially for small molecule aptamers [20]. Due to its homogeneous format, speed, accuracy and automated high-throughput capability, the fluorescent anisotropy aptamer assay has been used frequently to

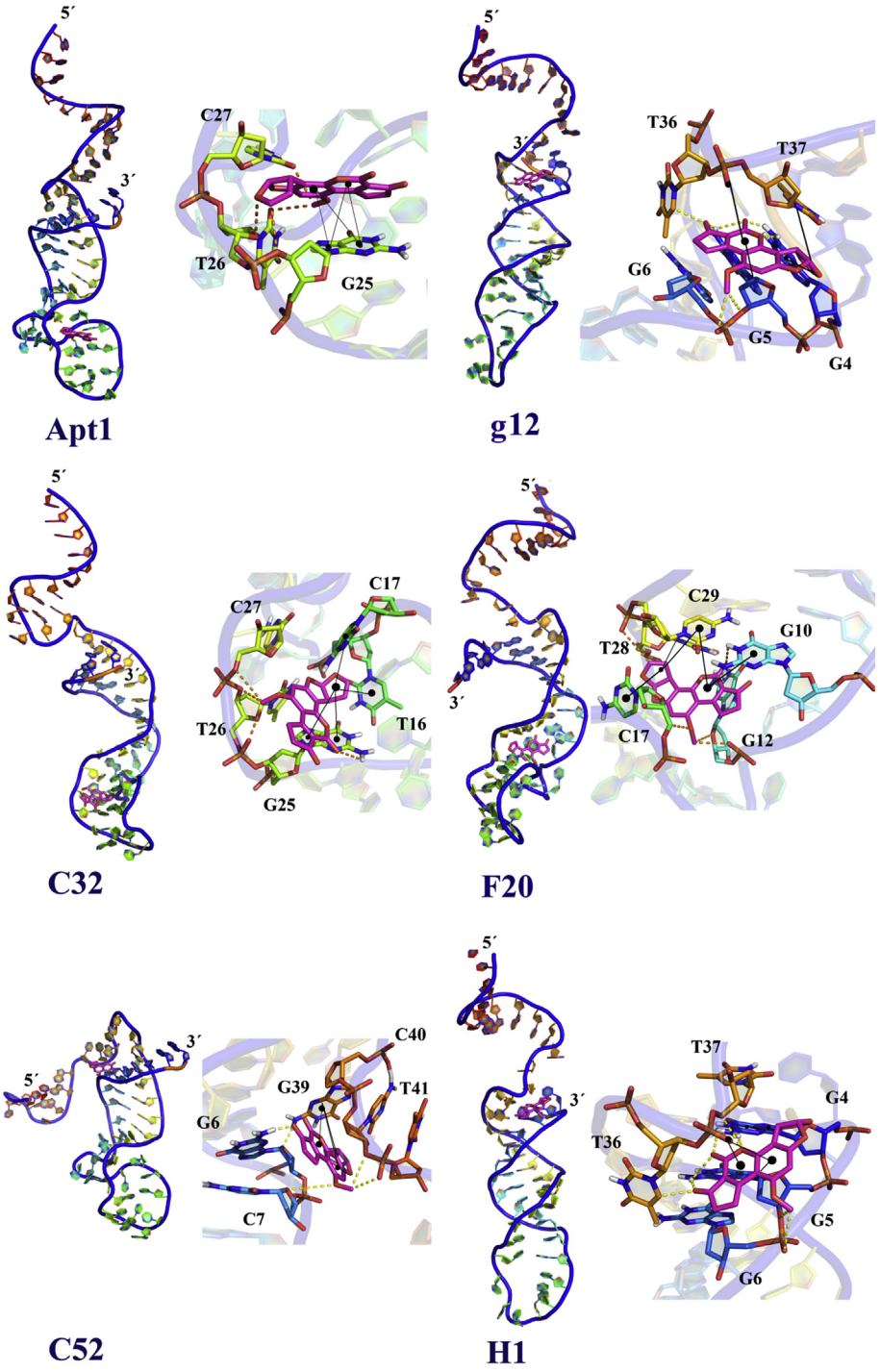

Fig. 2. The docking results of Apt1, C32,C52, g12, F20 and H1-aflatoxin B_1 complexes and residues involved in binding interaction in 3D representation. Dashes represent Carbone and conventional hydrogen binding, black dots and line represent electrostatic and hydrophobic interactions.

detect various small molecules [20,22,27]. In this study, a novel direct FAAA was designed based on the intrinsic fluorescence of AFB_1 instead of using a fluorescent-labeled aptamer. According to our hypothesis, AFB_1 molecules accumulated in the hydrophilic binding buffer as a large fluorophore and their fluorescence emission significantly decreased due to self-quenching. The large fluorophore of multiple AFB_1 tumbled slowly and produces a high fluorescent anisotropy signal. Upon aptamer addition, several AFB_1 molecules bound to the aptamer so becoming able to emit fluorescence and tumble faster (Scheme 2). The results for all the aptamers under investigation showed that the fluorescent emission of AFB_1 increased and its fluorescence anisotropy signal decreased gradually by increasing the aptamer concentrations. The binding affinity constant (K_D) calculated via the FAAA were in the range 4.02E-03 to 1.02E-01 nM and aptamer F20 showed the highest tendency to bind AFB_1 with up to 9.4 fold improvement in affinity compared to the parent Apt1 aptamer (Fig S5). The parallel AFB_1 fluorescence intensity (FI) increase was also recorded and plotted

Table 1
Dissociation constant (K_D) values (nM) for the selected aptamers calculated by using three experimental methods (R^2~≥90) and comparison with the in silico approach. Aptamers are listed in descending order according to the in silico score. The lowest K_D value in each series is highlighted in bold.

Aptamer	Colorimetric assay	Fluorescent intensity assay	Fluorescent anisotropy assay	In silico score
F20	**8.70E+00**	2.34E-01	**4.02E-03**	**4.846154**
g12	2.25E+01	**2.13E-01**	1.92E-02	4.798859
C52	2.51E+01	2.82E-01	3.04E-02[a]	4.593767
Apt1	2.83E+01	2.94E-01	3.85E-02	4.45671
C32	2.13E+02	1.22E+01	5.24E-02	4.170306
H1	4.98E+01	3.41E+00	1.02E-01	3.445057

[a] The K_D value of aptamer C52 was calculated in the range 0–100 nm.

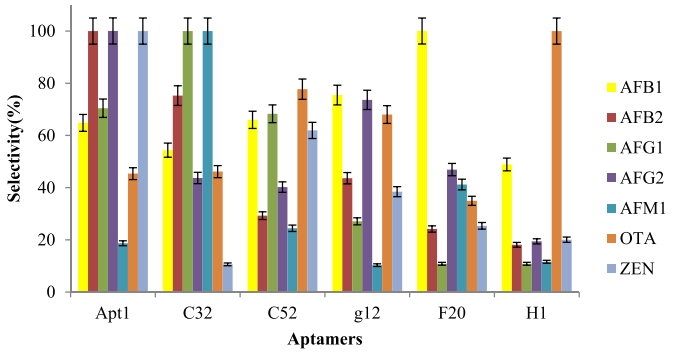

Fig. 3. Selectivity of the selected aptamers towards various mycotoxins (10 ng ml^{-1}) as measured by the colorimetric sensing approach.

versus the aptamer concentration. The FI method had lower sensitivity than the FAAA (~100 times) and the K_D values calculated by FI were in the range 2.13E-01 to 1.22E+01 nM (Table 1).

The order of binding affinity to AFB_1 calculated by the FAAA and the FI for the candidate aptamers was largely consistent (concordance 83.3% and 66.6% respectively) with the in silico results. It should be noted that the binding affinity of aptamer C52 decreased when the aptamer concentration was more than 100 nM. The 3D structure of aptamer C52 significantly differed from other aptamers that probably led to different functional properties in higher concentrations.

According to the results, the K_D of each aptamer measured using three different analytical approaches including unmodified AuNPs-based colorimetric assay, fluorescent intensity and direct fluorescent anisotropy aptamer assay were inconsistent. This finding is in line with a prior study that performed a comprehensive analysis of a panel of conventional affinity binding assays for small molecule aptamer evaluation and highlights their inconsistency. Due to the lack of standardized analytical methodologies for the characterization of small molecule-binding aptamers mainly related to the drastic different size between them and their small targets, it would be favorable to use multiple assays [20]. Regarding the inconsistency of different analytical methods, we applied multiple strategies (three different analytical methods) to overcome this problem and faithfully compared different aptamers based on binding affinity over AFB_1.

4. Conclusion

In the present study, we successfully coupled ISM with molecular docking to improve affinity and selectivity properties of the aptamer Apt1, previously developed towards AFB_1. The high consistency of the in silico results with the experimental findings confirmed that this strategy is a promising tool in order to design or optimize new functional aptamers. The computational methodologies facilitate the selection or improvement of desired aptamers by clarifying the interaction between ligand and receptor at the molecular level. However, the lack of specialized software for 3D structure prediction of ssDNA is an important constrain for in silico studies. The presented new pipeline can predict faithfully the tertiary structure of DNA aptamers from their sequence. For the first time, the 3D structure, binding sites and type of interactions of the known aptamer (Apt1) with AFB_1 was predicted and found to be in line with experimentally findings from other studies [27]. In addition, the analysis of different aptamer-AFB_1 complexes revealed that the lower binding energy, simpler secondary structure, lower ΔG, appropriate loop size (~12–20 bases), binding

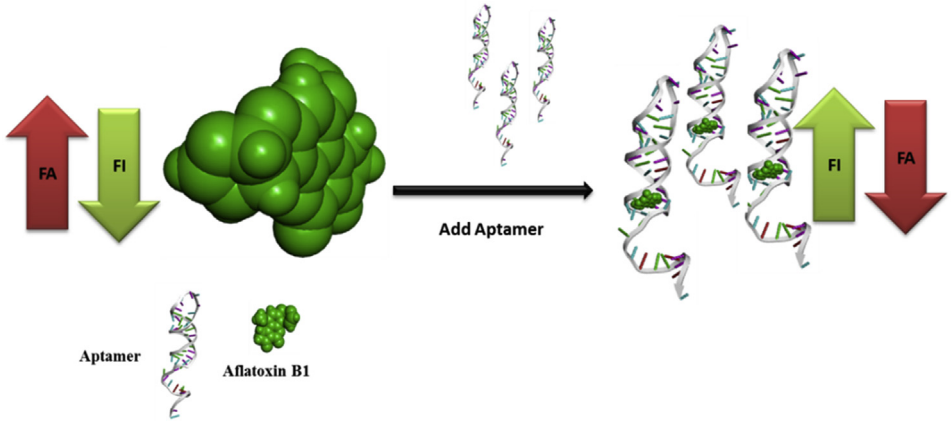

Scheme 2. Schematic representation of the direct Fluorescent Anisotropy Aptamer assay: AFB_1 molecules aggregated in the hydrophilic binding buffer as a large fluorophore with high fluorescence anisotropy (FA) and low fluorescence intensity (FI) due to self-quenching. Upon aptamer addition, AFB_1 molecules dissociated from the aggregate and interact with the aptamer. Accordingly, the anisotropy signal decreased and fluorescent intensity increased.

pocket and type of interactions can be considered as important factors in the selection of high affinity and selectivity aptamers.

Regarding methods to check aptamers affinity towards AFB_1, FAAA displayed the highest sensitivity. Also, FAAA is less prone to interference from the composition of binding buffers and organic solvents compared to the colorimetric assay. The same advantages shown by FAAAs in the characterization of small molecule binding aptamers [20,27], can be exploited to develop efficient fluorescent anisotropy aptamer-based biosensors.

Other strategies for aptamer improvement including conjugation of binding motifs for construction of multivalent aptamers, stabilization of aptamer structures or introduction of hydrophobic moieties into aptamers can be studied in the future through the proposed pipeline.

Declaration of competing interest

The authors declare that they have no known competing financial interests or personal relationships that could have appeared to influence the work reported in this paper.

CRediT authorship contribution statement

Maryam Mousivand: Conceptualization, Methodology, Validation, Formal analysis, Investigation, Writing - original draft. **Laura Anfossi:** Conceptualization, Methodology, Writing - review & editing, Supervision, Project administration, Funding acquisition. **Kowsar Bagherzadeh:** Methodology, Writing - review & editing. **Nadia Barbero:** Methodology, Writing - review & editing. **Amir Mirzadi-Gohari:** Methodology. **Mohammad Javan-Nikkhah:** Conceptualization, Methodology, Writing - review & editing, Supervision, Project administration, Funding acquisition.

Acknowledgments

This work was supported by Department of Plant Protection, College of Agricultural Sciences & Engineering, University of Tehran (Karaj, Iran) and Department of Chemistry, University of Turin, Via Giuria, 7 (Turin, Italy).

Appendix A. Supplementary data

Supplementary data to this article can be found online at https://doi.org/10.1016/j.aca.2020.01.045.

References

[1] F. Kang, Y. Ge, X. Hu, C. Goikavi, M.G. Waigi, Y. Gao, W.J. Ling, Hazard Mater 320 (2016) 80–87.
[2] A. Anttila , R.V. Ghat , J. Bond , S.J. Borghoff , F. X. Bosch , et al. International Agency for Research on Cancer, (2002) 169–366.
[3] S.M. Herzallah, Food Chem. 114 (2009) 1141–1146.
[4] B. Huanga, Z. Hanb, Z. Caia, Y. Wub, Y. Rena, Anal. Chim. Acta 662 (2010) 62–68.
[5] L. Anfossi, G.D. Arco, M. Calderara, C. Baggiani, C. Giovannoli, G. Giraudi, Food Addit. Contam. 28 (2011) 226–234.
[6] S.R. Garden, N.J.C. Strachan, Anal. Chim. Acta 444 (2001) 187–191.
[7] A. P. Wacoo, D. Wendiro, P. C. Vuzi, J. F. Hawumba, J. Appl. Chem. https://doi.org/10.1155/2014/706291.
[8] J. Qian, C.C. Ren, C.Q. Wang, W. Chen, X.T. Liu, H. Li, Q. Liu, N. Hao, H.M. Li, K. Wang, Anal. Chim. Acta 1019 (2018) 119–127.
[9] A.D. Ellington, J.W. Szostak, Nature 355 (1992) 850–852.
[10] G. Mayer, M.S. Ahmed, A. Dolf, E. Endl, P.A. Knolle, M. Famulok, Nat. Protoc. 5 (2010) 1993–2004.
[11] D.E. Goldberg, Addison-Wesley, Reading, MA. 1989.
[12] H. Hasegawa, N. Savory, K. Abe, K. Ikebukuro, 21(2016) 421; doi:.10.3390/molecules.21040421.
[13] K. Ikebukuro, Y. Okumura, K. Sumikura, I. Karube, Nucleic Acids Res. 33 (2005) e108.
[14] A. Bini, M. Mascini, M. Mascini, A. Turner, Biosens. Bioelectron. 26 (2011) 4411–4416.
[15] A. Ruscito, M.C. DeRosa, Front Chem 4 (2016), https://doi.org/10.3389/fchem.2016.00014.
[16] T. Fukaya, K. Abe, N. Savory, K. Tsukakoshi, W. Yoshida, S. Ferri, K. Sode, K. Ikebukuro, J. Biotechnol. 212 (2015) 99–105.
[17] B.Q. Li, Y.C. Zhang, G.H. Huang, W.R. Cui, N. Zhang, Y.D. Cai, PloS One 9 (2014), e86729, https://doi.org/10.1371/journal.pone.0086729.
[18] Y. Chushak, M.O. Stone, Nucleic Acids Res. 37 (2009) e87, https://doi.org/10.1093/nar/gkp408.
[19] I. Jeddi, L. Saiz, Sci. Rep. 7 (2017) 1178, https://doi.org/10.1038/s41598-017-01348-5.
[20] M. McKeague, A.D. Girolamo, S. Valenzano, M. Pascale, A. Ruscito, R. Velu, N.R. Frost, K. Hill, M. Smith, E.M. McConnell, M.C. DeRosa, Anal. Chem. 87 (2015) 8608–8612.
[21] Y. Luan, Z. Chen, G. Xie, J. Chen, A. Lu, C. Li, H. Fu, Z. Ma, J.J. Wang, Nanosci. Nanotechnol. 15 (2015) 1357–1361.
[22] J. Ruta, S. Perrier, C. Ravelet, J. Fize, E. Peyrin, Anal. Chem. 81 (2009) 7468–7473.
[23] Patent:PCT/CA2010/001292, NeoVentures Biotechnology Inch.
[24] W.B. Shim, H. Mun, H.A. Joung, J.A. Ofori, D.H. Chung, M.G. Kim, Food Contr. 36 (2014) 30–35.
[25] X. Guo, F. Wen, N. Zheng, Q. Luo, H. Wang, H. Wang, S. Li, J. Wang, Biosens. Bioelectron. 56 (2014) 340–344.
[26] W. Zheng, J. Teng, L. Cheng, Y. Ye, D. Pan, J. Wu, F. Xue, G. Liu, W. Chen, Biosens. Bioelectron. 80 (2016) 574–581.
[27] L. Sun, Q. Zhao, Talanta 189 (2018) 442–450.
[28] M. Zuker, Nucleic Acids Res. 31 (2003) 3406–3415.
[29] M. Popenda, M. Szachniuk, M. Antczak, K.J. Purzycka, P. Lukasiak, N. Bartol, R.W. Adamiak, Nucleic Acids Res. 40 (2012) e112, https://doi.org/10.1093/nar/gks339.
[30] E.F. Pettersen, et al., UCSF Chimera 25 (2004) 1605–1612.
[31] Molecular Operating Environment (MOE), 0901. By Chemical Computing Group Inc. (2014).
[32] W. Humphrey, A. Dalke, K.J. Schulten, Mol. Graph. 14 (1996) 33–38.
[33] G.M. Morris, R. Huey, W. Lindstrom, M.F. Sanner, R.K. Belew, D.S. Goodsell, A.J. Olson, J. Comput. Chem. 30 (2009) 2785–2791.
[34] W.L. DeLano, CCP4 newsletter, On Protein Crystallography 40 (2002) 82–92.
[35] D.S. Biovia, Discovery Studio Modeling Environment, Dassault Systemes, Release, San Diego, 2015, p. 4.
[36] J. Liu, Y. Lu, Nat. Protoc. 1 (2006) 246–252.
[37] N. Barbero, L. Napione, P. Quagliotto, S. Pavan, C. Barolo, E. Barni, F. Bussolino, G. Viscardi, Dyes Pigments 83 (2009) 225–229.
[38] J. Gevertz, H.H. Gan, T. Schlick, RNA 11 (2005) 853–863.
[39] J.M. Carothers, S.C. BOestreich, J.H. Davis, J.W. Szostak, J. Am. Chem. Soc. 126 (2004) 5130–5135.
[40] Commission, T.E. Commission, Regulation (EU) No 165/2010 of 26 February 2010 Amending Regulation (EC) No 1881/2006. O. J. L50/58-L50/12, 2010.